ELEVENTH EUROPEAN ROTORCRAFT FORUM

Paper No. 11

PERFORMANCE AND NOISE ANALYSES OF ADVANCED TURBO-PROP

Akira Azuma, Keiji Kawachi and Tadaaki Watanabe

Institute of Interdisciplinary Research
Faculty of Engineering, The University of Tokyo
Tokyo, Japan,

and

Yoshiya Nakamura

Ishikawajima-Harima Heavey Industry Co. Ltd.
Tokyo, Japan

September 10—13, 1985

London, England.

THE CITY UNIVERSITY, LONDON, EC1 V OHB, ENGLAND.

PERFORMANCE AND NOISE ANALYSES OF ADVANCED TURBO-PROP

Akira Azuma, Keiji Kawachi and Tadaaki Watanabe
University of Tokyo,

and

Yoshiya Nakamura
Ishikawajima-Harima Heavy Industry Co., Ltd.

ABSTRACT

The Local Circulation Method has been extended to analyze the performance and noise of Advanced Turbo-Prop (ATP). The analytical results on the performance of an ATP under the normal flight conditions are compared with the experimental data obtained by the wind tunnel test conducted at NASA Lewis Research Center, and shown to be in reasonable agreement with the experimental data.

In addition, the analyses are extended to get the variation of the airloading and the sound pressure under yawed flight conditions. It is shown that, as the sideslip angle increases, the time-wise variations of the aerodynamic bending moment acting on the blade and of the sound pressure near the propeller disk significantly increase.

Only small variations in the thrust and the torque are observed even in the case of the yawed flight, because the number of the blades is large and the frequency of the airloading is low.

Nomenclature

a	section lift curve slope, rad^{-1}
b	number of blades
C_{LD}	elemental blade design lift coefficient
C_P	power coefficient = $P/\rho n^3 D^5$
C_T	thrust coefficient = $T/\rho n^2 D^4$
C_Γ	parameter of bound vortex distribution
c	blade chord or speed of sound
D	propeller diameter
d	section drag
f	function defining blade surface
J	advance ratio = V/nD
ℓ	section lift
M	weighting matrix
M_B	aerodynamic bending moment
$(M_B)_{steady}$	aerodynamic bending moment at steady state

M_o	Mach number of flight speed = V_o/c
n	revolutions per second
P	power
P_{ij}	stress tensor
p	acoustic pressure
R	propeller radius
r	blade spanwise position or distance between observer and hubcenter
T	thrust or period of acoustic pressure wave = 1/n
t	time
U	inflow of blade section
$\vec{U}$	inflow vector of blade section
V	advancing speed = $V_o \cos \beta$
V_o	flight speed
$\vec{v}$	induced velocity vector
v_n	component of induced velocity normal to the plane of blade rotation or blade element velocity normal to blade surface
v_p	component of induced velocity perpendicular to the inflow $\vec{U}$
v_q	component of induced velocity parallel to the inflow $\vec{U}$
x_b	position of bound vortex nondimensionalized by the blade chord
x_c	position of control point nondimensionalized by the blade chord
y	space coordinate
y_c	position of control point nondimensionalized by R
β	sideslip angle
Γ	circulation
δ	elevation angle of observer position from rotor plane, $\delta = \sin^{-1}(z/r)$, or delta function
η	propeller efficiency = TV/P
θ	blade pitch angle
θ_t	blade twist angle
θ_o	blade pitch angle at 0.75R
κ	reduced frequency
ρ	air density
Φ	general inflow angle
ϕ	inflow angle
ψ	azimuth angle

INTRODUCTION

There are a few methods used to analyze the spanwise airloading acting on the ATP; vortex theory[1], acceleration potential theory[2], and finite-difference method solving Euler equations[3]. These methods of analysis are capable to evaluate the airloading precisely, but require the considerable computer time even in the steady axial flow. This sometimes leads to the limitation of the applicability of the calculation for the complex flow field, such as yawed flight, gust response, etc.

The local momentum theory[4] (LMT) was proposed as a practically useful tool for calculating effectively the time-wise variation of airloading of helicopter rotors. Furthermore, the local circulation method[5],[6] (LCM) was developed as an extension of the LMT in order to calculate the airloading of the rotary wings, such as propeller and wind turbine, operating in the high axial flow field.

It is indicated that the LCM has the capability of achieving a level of accuracy similar to that of the vortex theory, and of consuming much smaller computer time than that of the vortex theory.

By taking these advantages, the analysis of the aerodynamic forces and the sound pressure of the ATP will be presented here.

LOCAL CIRCULATION METHOD

The LCM used in this study is briefly explained here. More detailed explanations of the LCM are given in Refs. 5 and 6. In the LCM, the induced velocity is considered to be given rise at the time a blade hits the space, and vanishes gradually as time elapses corresponding to the development of the wake. The instantaneous bound vortex which makes the aerodynamic force at every instance is evaluated under the assumption that the trailing vortex flows straight to the direction of airflow. The time-wise change of induced velocity is simply expressed by multiplying the attenuation coefficient to the original value.

Fig. 1 illustrates the flow profile at an arbitrary section of blade. Trailing vortex filaments do not necessarily lie on a flat plane since the inflow angle to the rotational plane $\phi=\tan^{-1}(V/r\Omega)$ varies along the span.

Since the blade of the ATP is that of low aspect ratio and highly swept-back, Weissinger's so-called simplified lifting surface theory[7] (or the quasi-lifting surface theory) may be introduced in the LCM as follows: As shown in Fig. 2, a bound vortex is located on the quarter-chord line, $x_b=c/4$, and the control point, which is usually taken on the three-quarter chord, is given by

$$x_c=x_b+(a/4\pi)c \quad \ldots\ldots (1)$$

The boundary condition, that no flow penetrates into the blade considered to be a thin plate at the control point, is given by

$$\theta\cong(v_p/U)+\phi. \quad \ldots\ldots (2)$$

The actual blade is represented by a series of hypothetical wings of decreasing wing-span (Fig. 3). Each hypothetical wing has an elliptical distribution of circulation along the spanwise axis which is perpendicular to the inflow. The trailing vortices shed from this hypothetical wing are straight to the direction of the general inflow, and extended to infinity; therefore, the induced velocity at the control point of the hypothetical wing is calculated by analytical solution obtained from Biot-Savart law. The actual airloading and induced velocity distribution of a real blade is represented by the summation of the lift and induced velocity of this series of hypothetical wings. Therefore, by using the boundary conditions given by equation (2), the following equations of circulation is given:

$$(U_1\theta_1,\ U_2\theta_2,\ \ldots\ U_n\theta_n)^T = M \cdot (C_{\Gamma_1}, C_{\Gamma_2} \ldots C_{\Gamma_n})^T \quad \ldots\ (3)$$

where M is the $n \times n$ matrix, and is calculated by knowing only the planform of the blade. The matrix M becomes a triangular matrix by neglecting the induced velocity outside every hypothetical wing, and equation (3) is solved without calculating the inverse matrix or introducing any iterations.

In order to take the induced velocity due to the preceding wing into account, an "attenuation coefficient" is introduced. This coefficient represents the time-wise change of induced velocity at any local station due to the wake development into a spiral form. Suppose a rotary wing which gives rise to an induced velocity or momentum change at the very moment it passes a space of interest. This induced velocity is taken as the effect of the preceding wing with respect to the succeeding wing and decreases in value as time elapses by multiplying the attenuation coefficient C. Thus, the following wing is considered to go through the induced velocity field of Cv. Then, the general inflow velocity is considered to be given by the sum of wind velocity (advancing velocity), rotational velocity, and the induced velocity made by the preceding wings.

The attenuation coefficient can be calculated by assuming a simple wake model. Two components of the induced velocity should be taken into account; one is perpendicular to the rotational plane and the other is in that plane.

The experimental data of the wing section can be utilized in the LCM. The control point moves corresponding to the section lift curve slope as shown in equation (1). Therefore, the effects of the compressibility and the stall are taken into calculation through the experimental airfoil data. The chart of the airfoil data for NACA 16 series is used in this calculation, because the SR-3 model[8] is exemplified.

In this analysis, the effect of the shed vortices on the instantaneous generation of the induced velocity and on the attenuation coefficient are ignored. The former leads to the introduction of the quasi-steady assumption, $\kappa=0$. The effect of the shed vortices of the preceding blades is, however, taken into calculation as the time-wise change of the induced velocity left in the rotational plane.

RESULTS AND DISCUSSION

In order to examine the ability of the LCM extended to the analyses of the ATP, the performance for the steady axial flow is analyzed. The exemplified ATP is the SR-3 model, the geometry and the operating conditions of which are given in Figs. 4(A) and (B).[8] The inflow and coordinate system are indicated in Fig. 4(C). The computational results of the performance are shown in Fig. 5(A) for constant pitch, constant advance ratio and constant efficiency. These analytical results are compared with the wind tunnel test,[8] as shown in Fig. 5(B). It is apparent that the LCM gives very reasonable prediction of the ATP performance. Only small difference between the experiment and the analysis is observed when the advance ratio, $J=V/nD$, is small.

Because the advancing speed, V, is constant in this experimental test, this difference is observed when the rotational speed increases. Therefore, the difference might be caused by the blade elastic deformation, specifically torsional deformation, by the strong centrifugal force.

Shown in Fig. 6 are examples of the spanwise distribution of angle of attack for the various advance ratio. Although the pitch angle, $\theta_o=59.3°$, and the twist angle, $\theta_t \fallingdotseq -30°$, are very large, the inflow angle cancels these values, and the resultant angle of attack is small. This means that the estimation of the induced velocity distribution is still important for high axial flow field.

In order to analyze the effect of the yawed flight, (effect of sideslip or effect of angle of attack of the propeller shaft), a set of flight condition specified by the pitch angle of $\theta_o = 59.3°$ and the advance ratio of $J=3.44$, which gives the best efficiency for the steady axial flow as shown in Fig. 5(A), was selected. The effect of the sideslip angle (or the angle of attack) on the performance, the mean value of the thrust coefficient versus the torque coefficient, is shown in Fig. 7. It is observed that the both coefficients increase with the sideslip angle.

The spanwise and azimuth-wise distributions of the angle of attack in the yawed flight are also shown in Figs. 8(A) and 8(B). It can be seen from these figures that, as the sideslip angle increases, the time-wise or azimuth-wise variation of the angle of attack increases with the frequency of once per revolution. This is essentially caused by the variation of the inflow angle. Therefore, the forces generated by the respective blade are cancelled each other, and the variation of the total forces and moment such as the thrust and the torque are very small even in yawed flight.

Small fluctuations of the angle of attack with the high frequency are also observed in the advancing side of the blade ($0° \leqq \psi \leqq 180°$). This is caused by the change of induced velocity generated by the preceding blade, specifically at its tip. However, since the time step of computation is equivalent to the azimuth-wise step of $\Delta\psi=5°$, only the frequency of the variation expressed by this time step is reliable.

The variation of the aerodynamic bending moment about the blade root is shown in Fig. 9. The value is normalized by the

bending moment of the axial flow without sideslip angle, $(M_B)_{steady}$. It is clearly observed that the aerodynamic bending moment significantly increases with the sideslip and its frequency is that of one per revolution. Therefore, the blade rigidity must be determined to bear the above high bending moment, even if the aerodynamic moment variation acting on the rotating shaft is small.

APPLICATION TO THE NOISE PREDICTION

1) Description of the Prediction Method

Based on the above results of the angle-of-attack distribution, which has been obtained in 3-D manner by incorporating the induced flow effect from other blades, the sectional pressure distribution on the blade is calculated by Moriya's method[9] of successive conformal mapping. Then the ATP acoustic field can be obtained by applying the well-known Ffowcs Williams-Hawkings equation[10]:

$$\Box P \equiv \frac{1}{c^2}\frac{\partial^2 P}{\partial t^2} - \nabla^2 P = \frac{\partial}{\partial t}\{\rho_0 v_n |\nabla f| \delta(f)\} - \frac{\partial}{\partial y_i}\{P_{ij}\frac{\partial f}{\partial y_j}\delta(f)\} \quad \ldots(4)$$

The acoustic sources on the blade surfaces are integrated for the retarded time which is given by the source and observer motions. Therefore, the assumptions used in the present paper are as follows:

i) Isolated rotor in the uniform flow field without any sound reflection nor diffraction.
ii) Two dimensionality of the local blade element pressure distribution for given angle of attack.
iii) Invicid and incompressible flow with Prandtl-Glauert type correction.
iv) Non-compact linear acoustic source excluding quadruple term.

These assumptions limit the range of applicability of this prediction method to a single rotor operating in subsonic range.

2) Results and discussion

Fig. 10 shows an example of acoustic pressure waveform generated by any single blade during one revolution and the "influential surface" at different observer times. The rotor geometry and operating conditions are same as those described in Fig. 4. The observer locates at $\psi=180°$, $\delta=30°$, ahead of rotor plane with distance of three times of rotor diameter from the hub center. The observer will receive the pressure wave emitted from all sources distributed on the influential surfaces and hear it as sound. It can be seen that the influential surface of the approaching blade ($0°<\psi<180°$) towards the observer is elongated (having longer apparent chord length), whereas the retreating blade ($180°<\psi<360°$) is shrinked (less chord length) by the blade motion.

Because the acoustic pressure is proportional to the multiple of source intensity and the source area (influential surface area) in the near field, or proportional to its time

derivative in the far field, the dominant fluctuation of acoustic pressure is likely to occur at the observer time corresponding to the instance when the influential surface area or its time derivative becomes maximum. This is around $\psi=90°$ where the large negative peak is observed actually in Fig. 10.

The total waveform generated by all blades of the propeller is obtained by summing up the waveform of the respective blades. Because each blade has equal inter blade phase angle, their waveform also has equal phase shift. As a result, the amplitude diminishes by great deal due to the cancellation effect as shown in Fig. 11.

Fig. 12 shows the peak to peak acoustic pressure amplitude against (A) sideslip angle and (B) observer axial position.

The unsteady fluctuation of aerodynamic force induced on the blade due to sideslip makes increased acoustic pressure amplitude as shown in Fig. 12(A). This tendency is similar to Padula et al's prediction for the SR-2 propeller with shaft angle of attack[11], but the increasing rate with the angle is much larger than that of Ref. 11.

It is hard to identify the reason for this difference because the many parameters such as blade geometry or operating conditions are different. However the difference of aerodynamic code as an input to the noise calculation could be probable.

The primary propagating direction is elevation angle of $\delta=-10°\sim-15°$, behind the rotor plane manifested in Fig. 12(B), and this result is similar to Padula et al's. This primary angle is generally reasonable as the loading noise generated by blade differential pressure propagates toward some angle behind the rotor whereas the thickness noise propagates toward rotor in plane most strongly.

CONCLUSION

The analysis based on the local circulation method (LCM) has been applied to calculate the performance of an advanced turbo-prop (ATP) operating in normal flow condition and compared with experimental data obtained by the wind tunnel test conducted at NASA Lewis Research Center. The result is shown to be in good agreement.

Then the analysis is extended to calculate the spanwise distribution of the angle of attack and of the airloading, aerodynamic bending moment and sound pressure in neighbourhood of the ATP operating in yawed flight conditions. As the sideslip angle increases the variations of the aerodynamic bending moment and the sound pressure also increase significantly, whereas the variations of the hub forces and moment, such as the thrust and torque, are small because of large number of the blades.

REFERENCES

1) J. P. Sullivan, The Effect of Blade Sweep on Propeller Performance, AIAA paper 77-716, June 1977.
2) D. B. Hanson, Compressible Helicoidal Surface Theory for Propeller Aerodynamics and Noise, AIAA Journal, Vol. 21,

No. 6, June 1983, p.p. 881-889.
3) L. J. Bober, et al., Prediction of High Speed Propeller Flow Fields Using a Three-Dimensional Euler Analysis, NASA TM 83065, January 1983.
4) A. Azuma and K. Kawachi, Local Momentum Theory and Its Applications to the Rotary Wing, J. of Aircraft, Vol. 16, No. 1, 1979, p.p. 6-14.
5) K. Nasu and A. Azuma, An Experimental Verification of the Local Circulation Method for a Horizontal Axis Wind Turbine, The 18th Inter Society Energy Conversion Engineering Conference, Orlando, Florida, Aug. 21-26, 1983.
6) K. Nasu, A Method of Computation for the Blade Loading of Rotary Wing, Ph.D. Thesis, Faculty of Engineering, The University of Tokyo, 1983.
7) J. Weissinger, The Lift Distribution of Swept-Back Wings, NACA TM 1120, 1947.
8) C. Rohrback, et al., Evaluation of Wind Tunnel Performance Testings of an Advanced 45° Swept Eight-Bladed Propeller at Mach Numbers From 0.45 to 0.85, NASA CR 3505, 1982.
9) T. Moriya, Fundamental aerodynamics, Baifukan, Tokyo, 1959, in Japanese.
10) J. E. Ffowcs Williams and D. L. Hawkings, Sound Generation by Turbulence and Surfaces in Arbitrary Motion, Philosophical Transactions of the Royal Society of London, Series, A, Vol. 264, 1969, p.p. 321-342.
11) S. L. Padula, and P. J. W. Block, Predicted Changes in Advanced Turboprop Noise with Shaft Angle of Attack, AIAA 84-2346, 1984.

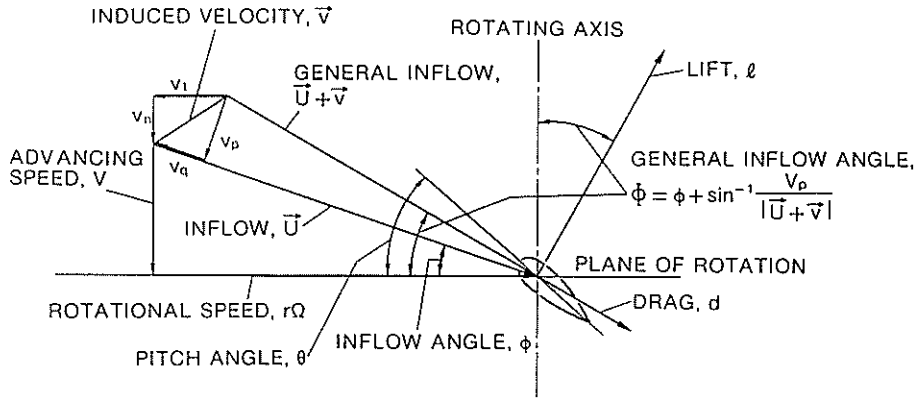

Fig. 1 Airflow and force configuration.

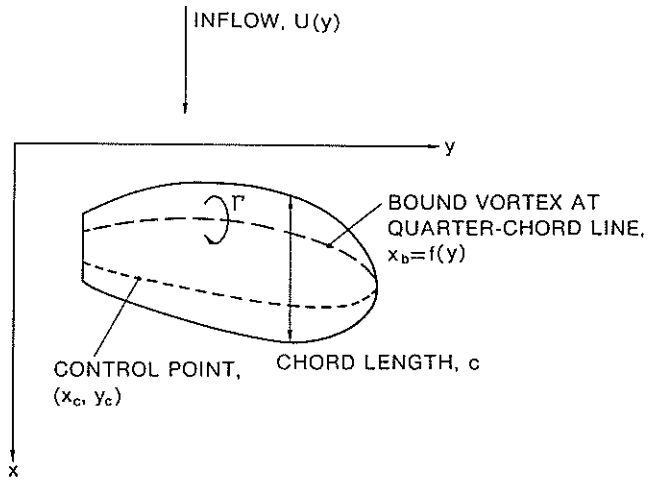

Fig. 2 Bound vortex and control point

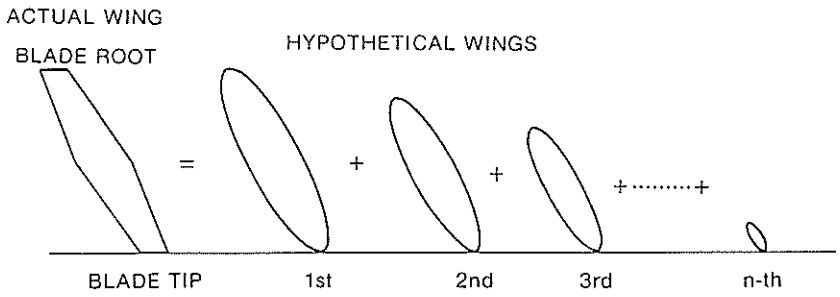

Fig. 3 Decomposition of a wing into hypothetical wings.

NUMBER OF BLADES, b=8
REVOLUTIONS, n=73~108 r.p.s.
ROTOR RADIUS, R=0.31m
MACH NUMBER OF FLIGHT SPEED, M_0=0.6
BLADE PITCH ANGLE, θ_0=59.3°~63.3°

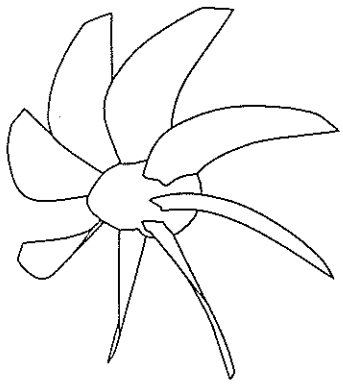

(A) SR-3 model

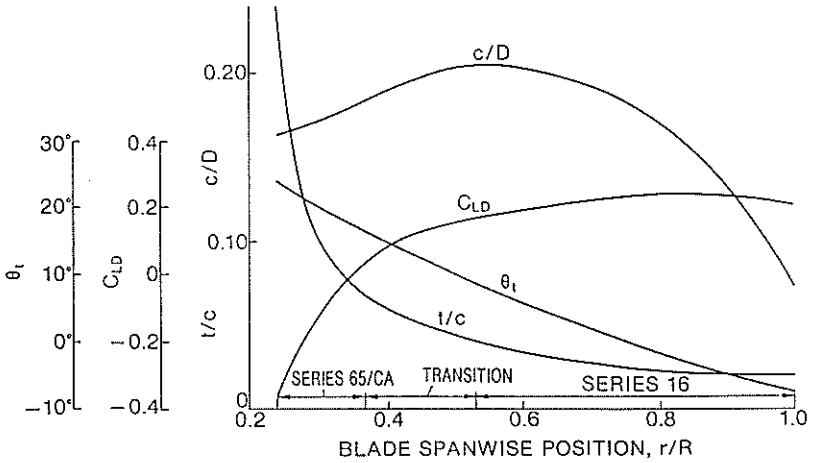

(B) Blade characteristics[8)]

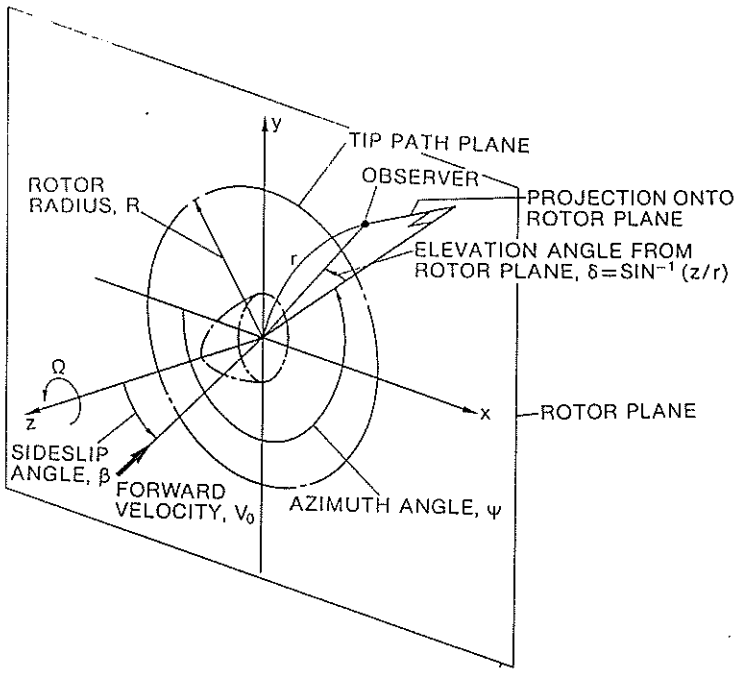

(c) Inflow and coordinate system

Fig. 4 Coordinate system and geometries

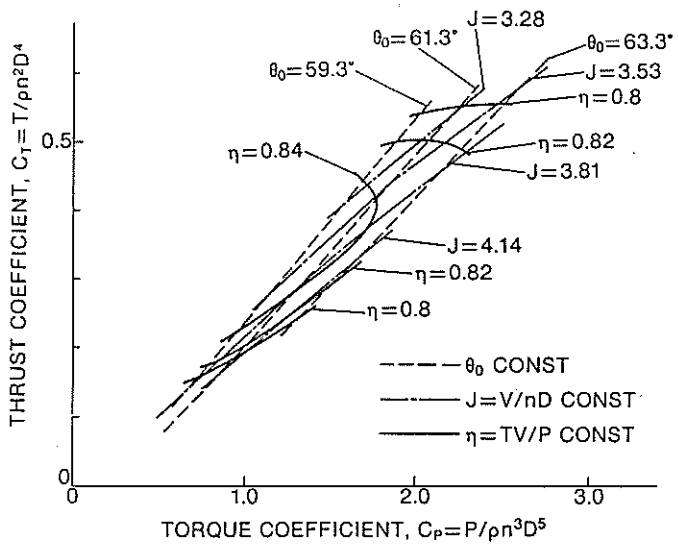

(A) Analytical result

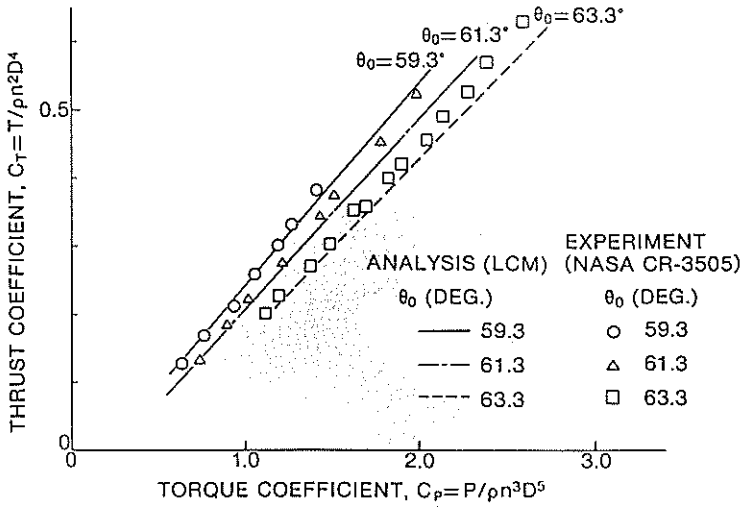

(B) Comparison of measured and calculated performance

Fig. 5 The performance of ATP ($\beta=0°$, $M_0=0.6$)

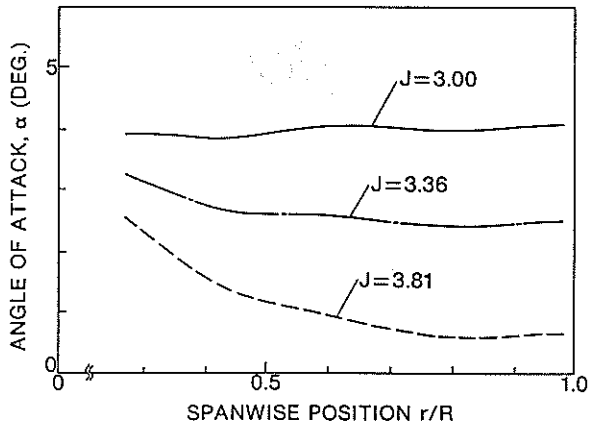

Fig. 6 Spanwise distribution of angle of attack ($\theta_0=59.3°$, $\beta=0°$)

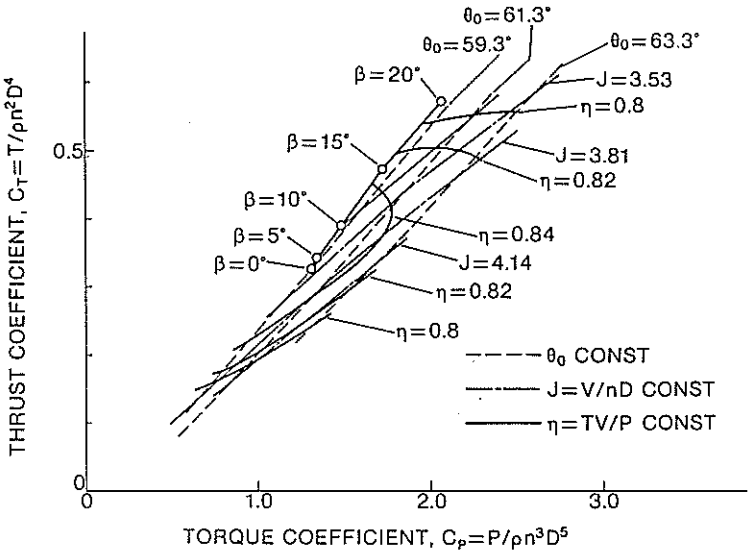

Fig. 7 Effect of sideslip angle on performance
(θ_0=59.3°, M_0=0.6)

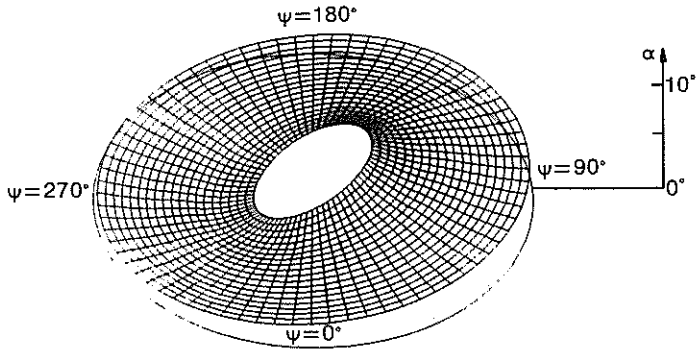

(A) β=5°

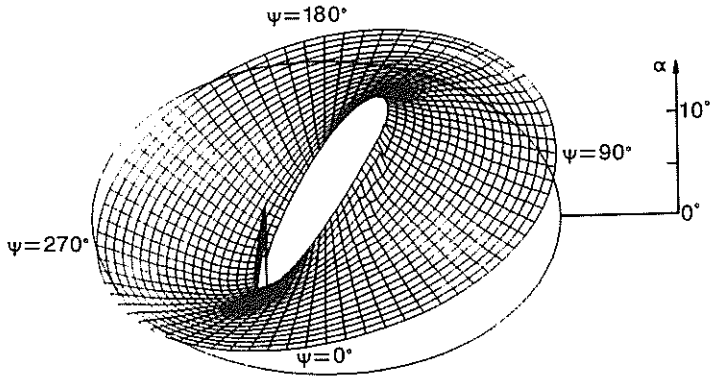

(B) β=15°

Fig. 8 Distribution of angle of attack in yawed flight
(θ_0=59.3°, M_0=0.6)

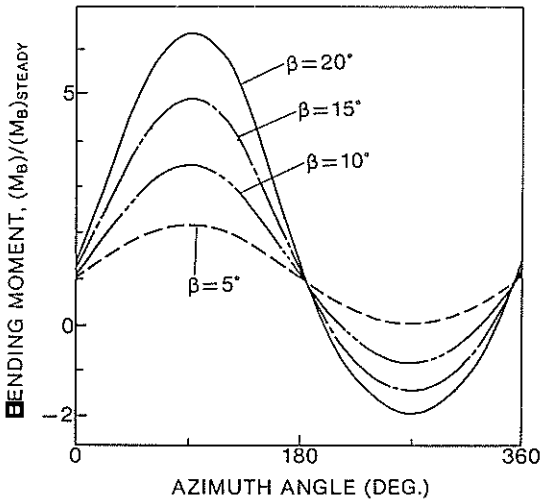

Fig. 9 Variation of aerodynamic bending moment in yawed flight (θ_0=59.3°, M_0=0.6)

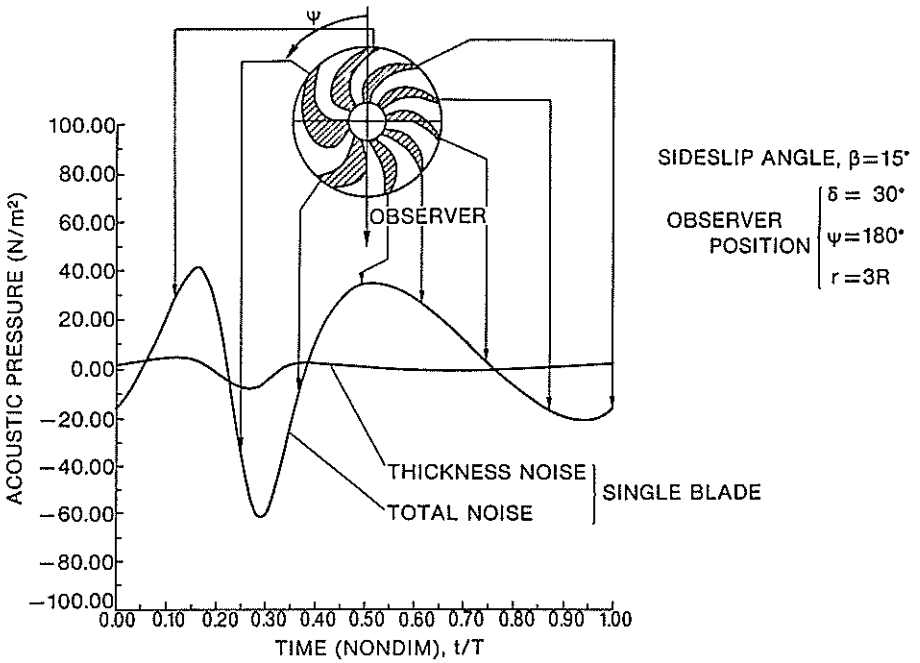

Fig. 10 Examle of calculated acoustic waveform and influential surface of single blade

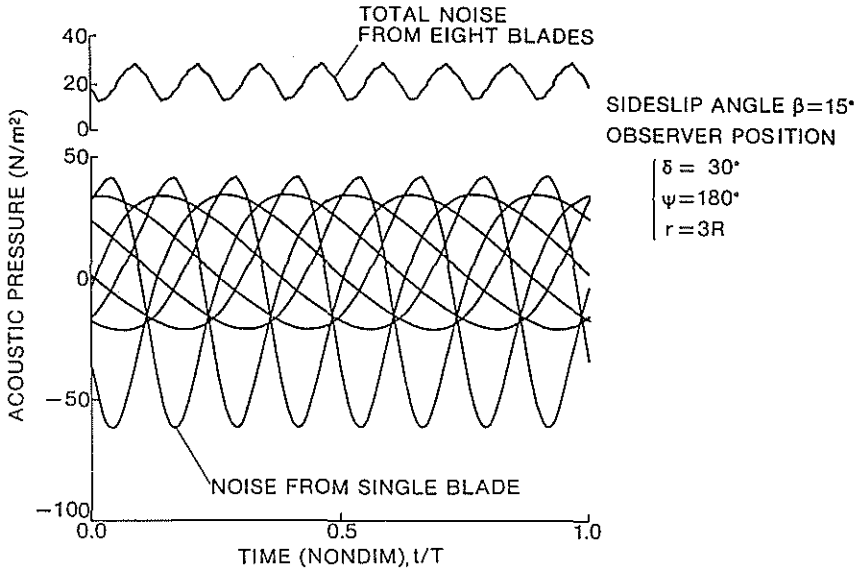

Fig. 11 Summation of eight waveforms from respective blades

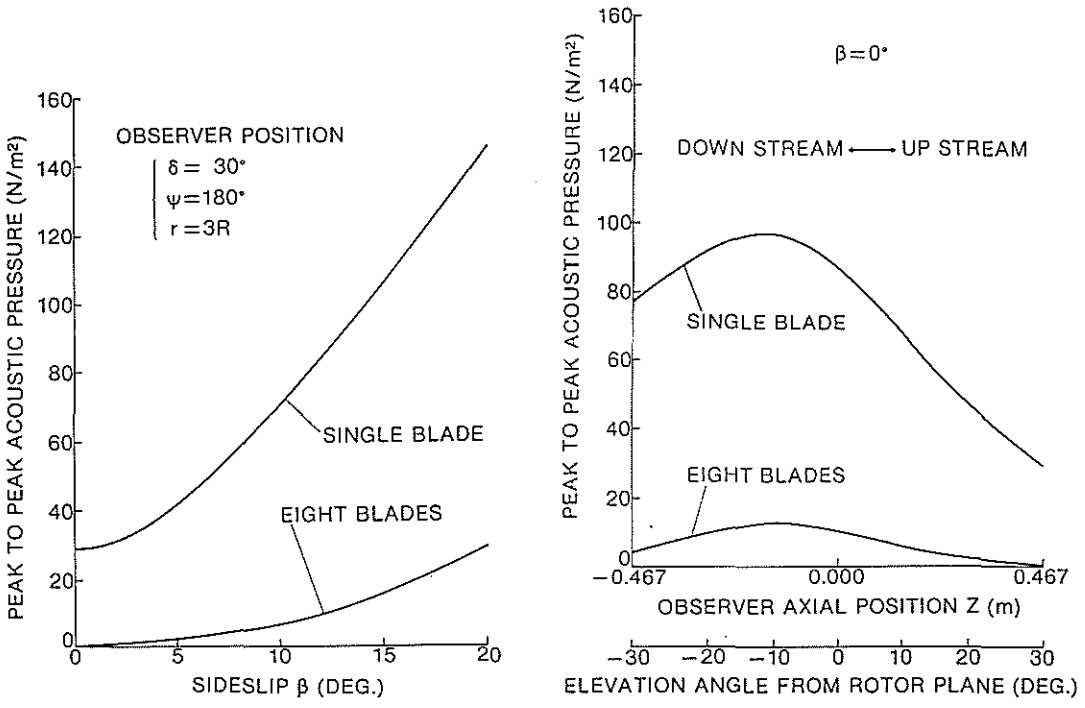

(A) Effect of sideslip

(B) Effect of elevation angle

Fig. 12 Peak to peak acoustic pressure